Superconducting cat qubits and their relatives

Filippos Dakis
Department of Physics, Virginia Tech, Blacksburg, Virginia 24061, USA
(Dated: December 7, 2023)

Contrary to a single two-level system, a cavity can store multiple excitations and coherences provided one can generate and manipulate coherent states. We present multiphoton control by using an artificial two-level system coupled to a waveguide cavity resonator in the strong dispersive regime. We propose a set of entangling gates that can create cat states in the resonator in the limit where the dispersive interaction is dominant compared to decoherence rates and higher-order nonlinearities. We go through the stabilization of cat states in a biased two-photon bath while also utilizing quantum Zeno effect to perform single qubit gates.

I. INTRODUCTION

Cavity and circuit quantum electrodynamics (cQED) are two testbeds for quantum optics, allowing the observation of strong interactions between photons and (artificial) atoms [1, 2]. These systems are exploited for the creation of highly non-classical states of light, such as cat states, with very interesting features that can be used in quantum computation and quantum communications. A cavity resonator, acting as a quantum harmonic oscillator (QHO) with infinite Hilbert space, is a promising candidate for storing multiple quantum bits or redundantly encoding information as it is necessary for quantum error correction (QEC). A QHO could be made equivalent to a multiqubit register, allowing for simplifications of hardware design [3, 4] and resource reduction. Creating non-classical states of light with many photos has been demonstrated [1], but actions must be taken to tackle photon dissipation and their short decoherence time [5] which are prerequisites for quantum computation. There have been theoretical proposals on stabilizing cat states by engineering the bath interacting with the system [6] followed by experiments verifying their effectiveness [7, 8]. Stabilizing cat states in a biased bath of single photon loss paves the way for using them in QEC schemes [4, 9].

The report is organized as follows. In Sec. II, we review and explain in detail the creation of cat states in a superconducting cavity utilizing the strong dispersive Hamiltonian and classical driving fields. In Sec. III we review the stabilization of coherent states in a biased bath of single and two-photon dissipation. In Sec. IV, we introduce an example to underline the potential of using cat states in QEC. Finally, in Sec. V, we propose some interesting directions that we could further investigate.

II. CATS AS QUBITS IN STRONG DISPERSIVE REGIME

Let us begin by considering a two-level system (TLS) [10] in a superconducting cavity in which the system evolves under the Jaynes–Cummings Hamiltonian

$$H_{\rm JC}/\hbar = \tilde{\omega}_c a^\dagger a + \frac{\tilde{\omega}_q}{2}\sigma_z + \mathrm{g}\left(\sigma a^\dagger + \sigma^\dagger a\right)\,, \tag{1}$$

where $\tilde{\omega}_{c,q}$ are cavity and TLS transition frequencies, g is the cavity-TLS coupling strength, $a^\dagger(a)$ are the raising (lowering) ladder operators of the cavity resonator, $\sigma_z = |e\rangle\langle e| - |g\rangle\langle g|$, and $\sigma = |g\rangle\langle \mathrm{e}|\ (|e\rangle, |g\rangle$ are the excited and ground states of the TLS). We are interested in the strong-dispersive regime where the TLS and the photon frequencies are highly detuned, i.e. $|\tilde{\omega}_c - \tilde{\omega}_q| = |\Delta| > \mathrm{g}$. For large Δ we expect the energy exchange, given by the last term in Eq. (1), to be suppressed, in other words, the cavity will not be able to excite the TLS and the TLS will not be able to emit a photon in the cavity. To eliminate the energy interaction term, we apply a Schrieffer-Wolff transformation using the operator $T = \exp\left[\frac{\mathrm{g}}{\Delta}(\sigma a^\dagger - \sigma^\dagger a)\right]$ and expanding to second order in g [11],

$$H_{\rm eff} = \frac{\hbar}{2}\left(\tilde{\omega}_q + \frac{\mathrm{g}^2}{\Delta}\right)\sigma_z + \hbar\left(\tilde{\omega}_c + \frac{\mathrm{g}^2}{\Delta}\sigma_z\right)a^\dagger a\,. \tag{2}$$

We can write the above Hamiltonian in a more compact form by using the $\omega_{c,q}$ as the renormalized cavity and TLS frequencies and shifting the overall energy by an irrelevant constant [1, 12]

$$H_{\rm eff}/\hbar = \omega_q\sigma^\dagger\sigma + \omega_c a^\dagger a - \chi\sigma^\dagger\sigma a^\dagger a \tag{3}$$

with $\chi = \mathrm{g}^2/\Delta \sim 2\pi(2-10)$MHz[13] being the effective second-order coupling known as the dispersive shift. This type of interaction produces a state-dependent shift in either the TLS or cavity transition frequency. We can make use of this conditional frequency shift to create TLS-cavity entanglement with two operations: conditional cavity phase shifts and conditional TLS rotations [1]. The conditional cavity phase shift can be described by moving to the interaction picture, $H_{\rm int} = -\hbar\chi\sigma^\dagger\sigma a^\dagger a$, and calculating the evolution operator

$$\begin{aligned}\mathrm{C}_\Phi = e^{-\frac{i}{\hbar}H_{\rm int}t} &= e^{i\chi t\sigma^\dagger\sigma a^\dagger a}\\ &= \mathbb{1}\otimes|g\rangle\langle g| + e^{i\Phi a^\dagger a}\otimes|e\rangle\langle e|\,.\end{aligned} \tag{4}$$

The above conditional phase shift $\Phi = \chi\tau$ is induced on the cavity state and appears due to the free evolution of the dispersive Hamiltonian for a time τ. For instance,

$$\mathrm{C}_\Phi\left[\,|\alpha\rangle\otimes\frac{|g\rangle+|e\rangle}{\sqrt{2}}\right] = \frac{|\alpha,g\rangle + |\alpha e^{i\Phi},e\rangle}{\sqrt{2}}\,, \tag{5}$$

where $|\alpha\rangle = e^{-|\alpha|^2/2}\sum_{n=0}\alpha^n/\sqrt{n!}\,|n\rangle$ is a coherent state ($|n\rangle$ is a Fock state) represented by a complex number α. With the above operator, we can entangle the TLS with a linear combination of coherent states, or equivalently, with a superposition of infinite Fock states. We will see later on how we can use this two-qubit gate to create cat states in the cavity and also perform Wigner tomography.

The second two-qubit gate, the conditional TLS rotation,

is a rotation on the TLS state conditional on the photon number of the cavity state. Recall that the TLS frequency depends on the state of the cavity, particularly on the number of photons in it. Thus, in order to obtain this operation, we can introduce a classical field on resonance with the m^{th} photon number frequency, $\omega_q^m = \omega_q - \chi m$. The Hamiltonian yields

$$H = H_{\text{eff}} + H_{dr} = H_{\text{eff}} + \sigma_y \left(\epsilon(t) e^{-i\omega_q^m t} + \epsilon^*(t) e^{i\omega_q^m t} \right) , \quad (6)$$

moving to interaction picture and applying the rotating wave approximation (RWA)

$$\tilde{H} = -\hbar\chi(a^\dagger a - m)\sigma^\dagger\sigma + \epsilon(t)\sigma_y \, , \quad (7)$$

where σ_y is the Pauli matrix, and the amplitude envelope $\epsilon(t)$ of the driving field has been taken real. We can write the above Hamiltonian in a block diagonal form

$$\tilde{H} = \hbar \sum_n \tilde{H}_n \left| n \right\rangle \left\langle n \right| = \hbar \sum_n \left\{ -\chi(n-m)\sigma^\dagger\sigma + \epsilon(t)\sigma_y \right\} \quad (8)$$

and we can proceed further by writing each block in a rotating frame

$$\tilde{H}_n = \sum_n \epsilon(t) e^{i\Delta_{n,m} t \sigma^\dagger\sigma} \sigma_y e^{-i\Delta_{n,m} t \sigma^\dagger\sigma} \, . \quad (9)$$

where $\Delta_{n,m} = \omega_q^n - \omega_q^m$. For a state containing exactly m photons, the above evolution will lead to a TLS rotation around y-axis

$$R_{\hat{y},\theta}^m = \left| m \right\rangle \left\langle m \right| \otimes e^{-i\frac{\theta}{2}\sigma_y} + \sum_{n \neq m} \left| n \right\rangle \left\langle n \right| \otimes \mathbb{1} \, , \quad (10)$$

with angle $\theta = 2\int_0^\tau \epsilon(t)\mathrm{d}t$. The effect of this Hamiltonian on all the other number states is discussed in Appendix 1.

Another operation we must be able to perform is the TLS rotations unconditional to the number of photons in the cavity. In the experiments with artificial atoms placed in cavities the two system are always coupled to each other [1, 7, 14]. Similarly, the dispersive interaction $\chi\sigma^\dagger\sigma a^\dagger a$ is always present and this means that any gate performed on the TLS will result in some non-zero TLS-cavity entanglement. We can use rewrite Eq. (8) as

$$\tilde{H} = \hbar \sum_n \left\{ -\frac{\chi}{2}(n-m)\sigma_z + \epsilon(t)\sigma_y \right\} , \quad (11)$$

and considering a constant amplitude ϵ over time τ we can obtain a block diagonal evolution operator

$$\begin{aligned} U(\tau) = \sum_n U_n(\tau) \left| n \right\rangle \left\langle n \right| &= \sum_n e^{-i\tau\{\frac{\chi}{2}(m-n)\sigma_z + \epsilon\sigma_y\}} \left| n \right\rangle \left\langle n \right| \\ &= \sum_n e^{-i\varphi_n \sigma_{\theta_n}} \left| n \right\rangle \left\langle n \right| \, , \end{aligned} \quad (12)$$

where $\varphi_n = \epsilon\tau\sqrt{1 + \left(\frac{(m-n)\chi}{2\epsilon}\right)^2}$ is the roation angle, $\sigma_{\theta_n} = \cos(\theta_n)\sigma_y + \sin(\theta_n)\sigma_z$, and $\theta_n = \arctan(\frac{m-n}{2\epsilon}\chi)$ defines the axis of rotation in the yz-plane. The above result allows one to write the photon-dependent propagator $U_n(\tau)$ explicitly in the TLS manifold and then use this relation to examine the operation's ability to rotate the TLS independently of the cavity state. It can be shown that this approach can achieve unconditional TLS rotations with fidelity $\mathcal{F} > 0.96$ over a Hilbert space $N = 20$ [1].

As it can be seen by the dispersive Hamiltonian in Eq. (3), the cavity transition frequency is dependent on the TLS state resulting in two spectral peaks at ω_c^g and ω_c^e representing the cavity transition frequency conditional to the TLS state. We are interested in displacing the cavity state conditional on the TLS state. To that end, we can introduce a classical driving field resonant to ω_c^e transition resulting in the Hamiltonian

$$\begin{aligned} H_d = \omega_q\sigma^\dagger\sigma + \omega_c a^\dagger a - \chi\sigma^\dagger\sigma a^\dagger a \\ + (a^\dagger + a)\left(\varepsilon(t) e^{-i\omega_c^e t} + \varepsilon^*(t) e^{i\omega_c^e t} \right) , \end{aligned} \quad (13)$$

where $\varepsilon(t)$ is the complex amplitude envelope of the driving field. Using the unitary transformation $T = e^{i\omega_c^e t(a^\dagger a \otimes \mathbb{1} + \mathbb{1} \otimes \sigma^\dagger\sigma)}$ to transform in the rotating frame of the field, and upon applying RWA the Hamiltonian yields to

$$\tilde{H}_d = (\omega_q - \omega_c^e)\sigma^\dagger\sigma + \chi\sigma\sigma^\dagger a^\dagger a + a^\dagger\varepsilon(t) + a\varepsilon^*(t) \, , \quad (14)$$

and moving to interaction picture

$$\tilde{H}_d^{int} = a^\dagger\varepsilon(t) e^{i\chi t\sigma\sigma^\dagger} + a\varepsilon^*(t) e^{-i\chi t\sigma\sigma^\dagger} \, . \quad (15)$$

The evolution operator is

$$U_d(\tau) = e^{\int_0^\tau \xi(t)a^\dagger - \xi^*(t)a\mathrm{d}t} \, , \quad (16)$$

where $\xi(t) = -i\varepsilon(t)e^{i\chi t\sigma\sigma^\dagger} = -i\varepsilon(t)e^{i\chi t|g\rangle\langle g|}$. Equation (16) looks like the displacement operator we wanted to obtain, $D(\beta) = e^{\beta a^\dagger - \beta^* a}$, however, $U_d(\tau)$ performs displacements on the cavity conditional on the TLS state. This selectivity is hidden in the integration of $\xi(t)$. In detail, a cavity drive envelope $\varepsilon(t)$ with a small spectral width $\sigma_\omega \ll \chi$ will be able to selectively perform a displacement $D(\alpha)$ conditioned on the TLS being in the excited state $|e\rangle$. In this limit, the amount of displacement when the TLS is in $|g\rangle$ will be proportional to the spectral component of the envelope $\varepsilon(t)$ given by the Fourier transform at frequency χ,

$$\int_0^\tau \xi(t)\mathrm{d}t \propto \int_0^\tau \varepsilon(t) e^{i\chi t}\mathrm{d}t \approx \hat{\varepsilon}\{\chi\} \, .$$

In the discussed limit, $\sigma_\omega \ll \chi$, the displacement is $\sim \hat{\varepsilon}\{\chi\} \simeq 0$. On the other hand, when the operator acts on the $|e\rangle$ state the cavity experiences the displacement operation with $\beta = -i\int_0^\tau \varepsilon(t)\mathrm{d}t$, recall that $e^{\alpha A} = 1 + \alpha A + (\alpha^2/2!)A^2 + \ldots$. So, in the limit of long pulses, one can achieve the entangling operator

$$D_\beta^e = \mathbb{1} \otimes e^{i\Psi} \left| g \right\rangle \left\langle g \right| + D(\beta) \otimes \left| e \right\rangle \left\langle e \right| \, , \quad (17)$$

where Ψ is an induced phase accumulated on $|g\rangle$ due to the AC stark effect [1]. The conditional cavity displacement D_β^e acting on a product state produces, $D_\beta^e\{|0\rangle(|g\rangle + |e\rangle)\} = e^{i\Psi}|0, g\rangle + |\beta, e\rangle$, an entangled TLS-cavity state (up to a normalization factor).

Carefully examining Eq. (16) one observes that unconditional displacements can be achieved too. Short ($1/\tau \gg \chi$) square-shaped displacement pulses can lead to unconditional

displacements with fidelity $\mathcal{F} > 0.99$ [1]. This operation can be explained in the same fashion as we did in the conditional case. Specifically, for very short pulses the integration of $\xi(t)$ will be independent of the state because $\int_0^\tau \varepsilon e^{i\chi t} \simeq \varepsilon\tau$, for $1/\tau \gg \chi$. At this point, we must notice that unconditional displacements are preferred because they are much faster, and, as we will see later on, conditional displacements can be produced by combining a conditional cavity shift C_π with simple displacement operations, $D^e_\beta = D(-\beta/2)C_\pi D(\beta/2)$. For more information and properties of the displacement operator see Appendix 3.

Now that we have all the building blocks we can create cat states and measure their Wigner function in the dispersive regime. The quantum circuit in Figure 1 depicts the protocol of mapping and measuring a TLS in a superposition of coherent states. Here follow the steps to create a symmetric

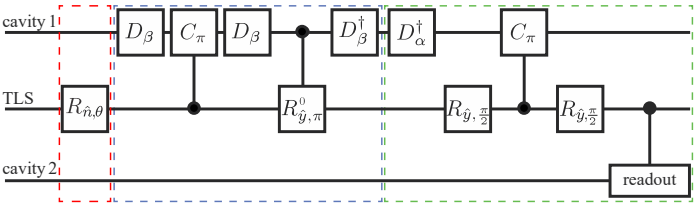

FIG. 1. Circuit diagram for the TLS initialization (red box), mapping of the TLS state to cavity (blue box), and cavity-state Wigner tomography (green box) using Ramsey interferometry with unconditional TLS rotations. Reproduced schematic from Ref. [1].

cat state starting from the initial state $|\psi_0\rangle = |0, g\rangle$

$$\begin{aligned} |0,g\rangle &\xrightarrow{R_{\hat{y},\pi}} |0\rangle \otimes (|g\rangle + |e\rangle) \xrightarrow{D_\beta} |\beta\rangle \otimes (|g\rangle + |e\rangle) \\ &\xrightarrow{C_\pi} |\beta, g\rangle + |-\beta, e\rangle \xrightarrow{D_\beta} |2\beta, g\rangle + |0, e\rangle \\ &\xrightarrow{R^0_{\hat{y},\pi}} (|2\beta\rangle + |0\rangle) \otimes |g\rangle \xrightarrow{D_{-\beta}} (|\beta\rangle + |-\beta\rangle) \otimes |g\rangle \\ &\equiv |\mathcal{C}^+, g\rangle \ . \end{aligned} \tag{18}$$

For convenience we disregarded the normalization factors in the above procedure. We chose to map the TLS $|+\rangle$ state to a superposition a symmetric superposition of macroscopically orthogonal coherent states $|\beta\rangle, |-\beta\rangle$ leading to the celebrated cat state $|\mathcal{C}^+\rangle = \mathcal{N}_+(|\beta\rangle + |-\beta\rangle)$, with $\mathcal{N}_+ = [2(1 \pm e^{-2|\alpha|^2})]^{-1/2}$. Notice that a coherent state is a classical state while the cat state is a quantum state. Note that one can map any TLS state to a superposition of coherent states only by changing the first TLS unconditional rotation and in this way one can encode the TLS information to the cavity and take advantage of infinite Hilbert space, for more see Sec. IV.

Wigner function provides precisely the same information stored in the density matrix but displays it in a very convenient and intuitive format [13]. Wigner quasi-probability distribution can be measured in a quantum non-demolition (QND) way by measuring the expectation value of the (displaced) parity operator in the following fashion [15]

$$W(\beta) = \frac{2}{\pi}\mathrm{Tr}\left\{\rho D^\dagger(-\beta)\Pi D(-\beta)\right\} , \tag{19}$$

where ρ is the cavity state density matrix and $\Pi = e^{i\pi a^\dagger a}$ is the parity operator (see Appendix 2). Note that measuring a field's Wigner function is a very powerful tool to investigate its non-classical properties, for more information, properties, and examples see Appendix 4 and Ref. [5]. To measure the Wigner function we adapt the recipe suggested in Ref. [5] or follow the circuit diagram (green box) in Fig. 1: prepare the cavity in a state ρ (we have already done that in the blue box), displace the cavity by an adjustable amplitude $-\alpha$, perform an Y gate, let the system evolve under the dispersive Hamiltonian for $\tau = \pi/\chi$, perform a Y gate, and measure the TLS using through a second cavity. Repeat the above process for all the phase space by adjusting the displacement amplitude $-\alpha$. To make it more clear, we observe that C_π is similar to parity

$$\begin{aligned} C_\pi = e^{i\pi a^\dagger a|e\rangle\langle e|} &= |g\rangle\langle g| + \Pi|e\rangle\langle e| \\ &= \Pi_+ \otimes \mathbb{1} + \Pi_- \otimes \sigma_z \, , \end{aligned} \tag{20}$$

and by applying Y-gates from both sides (as it is shown in Fig. 1) we obtain

$$YC_\pi Y = \Pi_+ \otimes \mathbb{1} - \Pi_- \otimes \sigma_x \, . \tag{21}$$

Thus if the photon number is even, nothing happens to the TLS, whereas if the photon number is odd the TLS is flipped. Hence we have successfully entangled the parity with the TLs state. Notice that starting with the TLS in the ground state, applying $YC_\pi Y$ and then measuring the state of the qubit reveals the parity expectation value at each point of the phase space but it does not measure the number of photons in the cavity. Figure 4 shows the Wigner functions for symmetric and antisymmetric "kitten" states (they are kitten states because the number of photons is low, $\bar{n} = 2.5^2$, and they cannot be considered cats).

III. PUMPED AND STABILIZED CAT QUBITS IN BIASED BATH

We discussed the very interesting case of strongly dispersive but we omitted the photon dissipation κ due to the finite cavity reflectivity, and also the TLS decay rate γ. Our analysis is a good approximation in the limit of $\chi \gg \bar{n}\kappa, \gamma$, but the full picture of the physics the system undergoes is captured via the master equation. Here we focus on the cavity density matrix and explore possible methods to create stabilized cat qubits in a biased bath.

If we solve the master equation for the reduced density matrix of the cavity state prepared in Sec. II we will witness its exponential decay to vacuum and thus the loss of the stored information, see Appendix 5. Educated by the asymptotic convergence of a periodically driven damped classical harmonic oscillator, we will try to stabilize our cat by driving our system. The master equation describing the single-photon driven QHO in a single-photon loss bath is [6]

$$\begin{aligned} \dot{\rho} = -i\omega_0\left[a^\dagger a, \rho\right] - i\epsilon_d\left[e^{-i(\omega_d t+\phi_d)}a^\dagger + e^{i(\omega_d t+\phi_d)}a, \rho\right] \\ + \kappa\mathcal{L}\left[a\right]\rho \, , \end{aligned} \tag{22}$$

where the first term is due to the QHO free energy, the second term represents the single-photon driving caused by a

classical field with amplitude $\epsilon(t)$ and frequency ω_d, and the $\mathcal{L}[a]$ is the Lindbland super-operator

$$\mathcal{L}[\mathcal{O}]\rho = \mathcal{O}\rho\mathcal{O}^\dagger - \frac{1}{2}\mathcal{O}^\dagger\mathcal{O}\rho - \frac{1}{2}\rho\mathcal{O}^\dagger\mathcal{O}\,. \tag{23}$$

To find the steady state solution we can apply a unitary transformation of the form

$$U(t) = D(-\bar{\alpha}e^{-i\bar{\phi}})e^{i\omega_d a^\dagger a}\,, \tag{24}$$

that transforms the system to the rotating frame of the driving field while displacing it by the amplitude obtained from the solution of the classical damped driven oscillator [6]. The transformed density matrix is $\tilde{\rho} = U(t)\rho U(t)^\dagger$ and the master equation yields

$$\dot{\tilde{\rho}} = -i(\omega_0 - \omega_d)\left[a^\dagger a, \tilde{\rho}\right] + \kappa\mathcal{L}[a]\,\tilde{\rho}\,, \tag{25}$$

which is the simply damped harmonic oscillator with steady state $\tilde{\rho}_{ss} = |0\rangle\langle 0|$, see Appendix 5. Transforming back we obtain

$$\rho_{ss}(t) = U(t)^\dagger\tilde{\rho}U(t) = |\alpha_{ss}(t)\rangle\langle\alpha_{ss}(t)| \tag{26}$$

with

$$\alpha_{ss}(t) = \bar{\alpha}e^{-i(\omega_d t+\bar{\phi})}\,, \quad \bar{\alpha}e^{-i\bar{\phi}_d} = \frac{-i\epsilon_d e^{-i\phi_d}}{i(\omega_a-\omega_d)+\kappa/2}\,. \tag{27}$$

Interestingly, the exponential convergence of the damped QHO to vacuum is translated to the exponential convergence of the periodically driven QHO to a pure coherent state defined by the driving and the photon dissipation. Although the above is an encouraging result, the steady state density operator spans only the one-dimensional Hilbert space which is not enough to stabilize a superposition of two coherent states.

One can follow the same procedure and find the steady states of multi-photon driven QHO in biased bath. As biased bath is considered a bath that extracts photons from the cavity in a specific way. For instance, the r-photon dissipation is caused by a biased bath, but the combination of an r-photon and an s-photon bath is not considered as biased. Consider the case of a two-photon driven dissipative QHO, the master equation in the rotating frame of the two-photon drive reads

$$\begin{aligned}\dot{\rho} &= -i\epsilon_2\left[e^{-i\phi_d}a^{\dagger 2} + e^{i\phi_d}a^2, \rho\right] + \kappa_2\mathcal{L}\left[a^2\right]\rho \\ &= \kappa_2\mathcal{L}\left[a^2-\alpha^2\right]\rho\,,\end{aligned} \tag{28}$$

where we assumed a resonant driving field ($\omega_0 = \omega_d$), and $\alpha_2 = e^{-i\phi_d/2}\sqrt{-2i\epsilon_2/\kappa_2}$. Any state in the kernel of the dissipation operator $a^2-\alpha^2$ is necessarily a fixed state of the above dynamics[6]. The fixed points of the dynamics are given by the solutions of the following equation

$$(a^2-\alpha^2)|\beta\rangle = 0 \Rightarrow \beta^2-\alpha_2^2 = 0 \Rightarrow \beta = \pm\alpha_2 \tag{29}$$

Comparing the above result with the one obtained in the single-photon drive dissipation process, we see that the fixed points here span a two-dimensional Hilbert space. It is worth mentioning that two-photon dissipation does not occur spontaneously. Instead, one has to engineer the bath or introduce this type of interaction through non-linear coupling [7, 8, 16].

For simplicity, assume a two-photon driving field such that the Hilbert space spanned by the ρ_{ss} is defined by $\mathcal{H}_2 = \text{Span}\{|-\alpha\rangle, |\alpha\rangle\}, \alpha \in \mathbb{R}$. Any linear combination of these two quasi-orthogonal states will be on the Bloch sphere. The logical qubit can be defined either by the symmetric and antisymmetric cats ($|\mathcal{C}^-\rangle, |\mathcal{C}^+\rangle$), or by the positive and negative coherent state ($|-\alpha\rangle, |\alpha\rangle$). It is shown that the first choice leads to a qubit exponentially robust under X (or phase-flip) errors, while the second choice leads to exponential suppression of the Z (or bit-flip) errors[17]. Both choices are vulnerable to single photon spontaneous jumps because $a|\mathcal{C}^\pm\rangle = \mp|\mathcal{C}^\pm\rangle$ and $a|\pm\alpha\rangle = \mp|\alpha\rangle$. For protection under the single-photon loss syndrome, the utilization of four-photon processes is required.

The map of the logical qubit to cat states is

$$|0\rangle = |\mathcal{C}^+\rangle \simeq \frac{1}{\sqrt{2}}(|\alpha\rangle + |-\alpha\rangle) + \mathcal{O}(e^{-2|\alpha|^2})\,, \tag{30a}$$

$$|1\rangle = |\mathcal{C}^-\rangle \simeq \frac{1}{\sqrt{2}}(|\alpha\rangle - |-\alpha\rangle) + \mathcal{O}(e^{-2|\alpha|^2})\,, \tag{30b}$$

see Fig. 2(c). For a qubit to be deemed practical and valuable for quantum computing, it must demonstrate the capability to undergo qubit rotations. A rotation or angle θ around logical X-axis is

$$\begin{aligned}X_\theta = &\cos(\theta)\left(|\mathcal{C}^+\rangle\langle\mathcal{C}^+| + |\mathcal{C}^-\rangle\langle\mathcal{C}^-|\right) \\ &+ i\sin(\theta)\left(|\mathcal{C}^+\rangle\langle\mathcal{C}^-| + |\mathcal{C}^-\rangle\langle\mathcal{C}^+|\right)\,.\end{aligned} \tag{31}$$

Note that even and odd cat states differ only in the way their fringes are distributed in phase space, see Fig. 4. So, to perform an X-gate, one must be able to shift between these two types of fringes. This can be done by a classical driving field pushing cat states along imaginary axis, $D(-i\varepsilon)$. The master equation is

$$\dot{\rho} = -i\varepsilon_x\left[a^\dagger + a, \rho\right] + \epsilon_2\left[a^{\dagger 2} - a^2, \rho\right] + \kappa_2\mathcal{L}\left[a^2\right]\rho\,. \tag{32}$$

Setting $\epsilon_2 = \bar{n}\kappa_2/2$ and $\alpha = \sqrt{\bar{n}}$ the above Zeno dynamics will occur in the space spanned by $\{|\mathcal{C}_\alpha^-\rangle, |\mathcal{C}_\alpha^+\rangle\}$ when $\epsilon_x \ll \kappa_2$[17]. The Zeno effect here refers to the exponential convergence of the system to $\mathcal{H}_2$, in other words, the system continuously projects itself on $\mathcal{H}_2$. Figure 2(a-b) presents the Rabi oscillations, and the Wigner function at different times obtained by solving Eq. (32) numerically with initial state $\rho(0) = |\mathcal{C}^+\rangle\langle\mathcal{C}^+|$. The system experiences an effective Rabi frequency $\Omega_x = 2\varepsilon_x\sqrt{\bar{n}}$ and, thus, by driving the system with a constant amplitude for time $\tau_x = \frac{\pi}{2\Omega_x}$ we perform an X-gate. The trajectory of the state is shown in Fig. 2(c). Furthermore, in Fig. 2(d) we present the state fidelity $\mathcal{F} = |\langle\mathcal{C}_{\tau_x}|\,|\mathcal{C}^-\rangle|^2$ sweeping over detuning the $\Delta = \omega_0 - \omega_d$ and the driving amplitude ε_x. The gate time is always $T_g = \frac{\pi}{2\Omega_x}$ revealing the already known trade-off between the gate time and the fidelity.

Continuing on the same idea of driven dissipative photon processes, the next logical step is to consider four-photon driving in the four-photon dissipative bath. In such case, the four-dimensional Hilbert space is spanned by 4 orthogonal cat states (symmetric and antisymmetric cats along real and imaginary axis, $|\mathcal{C}_\alpha^\pm\rangle, |\mathcal{C}_{i\alpha}^\pm\rangle$). With the right choice of logical qubit and by applying a quantum error correction (QEC) code, the single photon jumps can be tackled. For more information on this topic see Ref.[4, 17, 18]

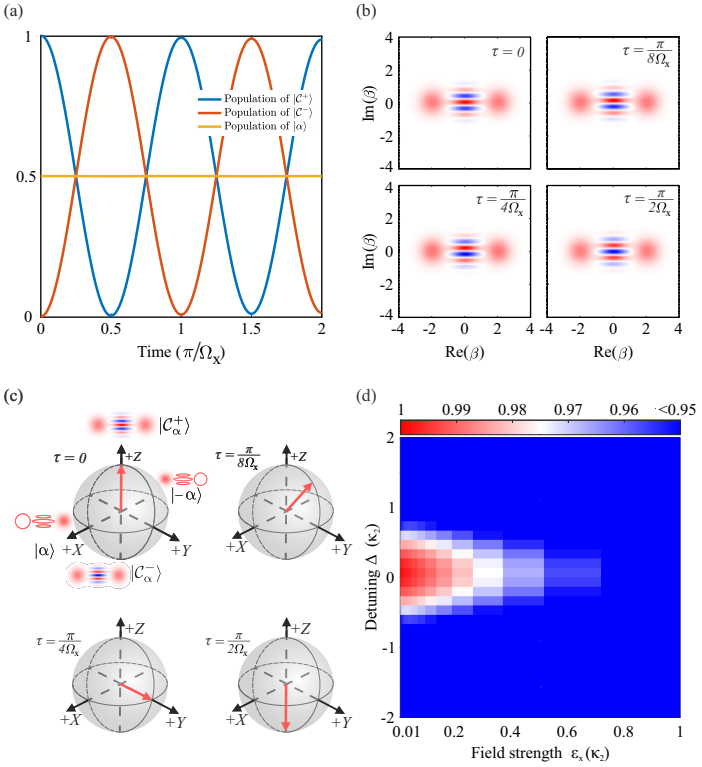

FIG. 2. Utilizing quantum Zeno dynamics to perform an X gate of the logical qubit space spanned by $\{|\mathcal{C}^+\rangle, |\mathcal{C}^-\rangle\}$. (a) Rabi oscillations around x-axis in the logical qubit space with effective Rabi frequency $\Omega_x = 2\varepsilon_x\sqrt{\bar{n}}$ ($\varepsilon_x = \kappa_2/20$, , $\bar{n} = 4$). (b) Wigner function at times $\tau = 0$, $\tau = \frac{\pi}{8\Omega_x}$, $\tau = \frac{\pi}{4\Omega_x}$, $\tau = \frac{\pi}{2\Omega_x}$ with the evident fringes shift. (c) State vector on Bloch sphere for the same times as in (b). (d) State fidelity $\mathcal{F} = |\langle \mathcal{C}_{\tau_x} | \mathcal{C}^- \rangle|^2$ over detuning $\Delta = \omega_0 - \omega_d$ and driving amplitude ε_x.

IV. APPLICATIONS IN QUANTUM ERROR CORRECTION

In this section we present how we can exploit the infinite and equidistant energy spectrum of a QHO to correct errors due to single-photon jumps. Assume that we can map an arbitrary TLS state $|\phi\rangle = c_g|g\rangle + c_e|e\rangle$ into a superposition of cat states $|\psi_0\rangle = c_g|\mathcal{C}_\alpha^+\rangle + c_e|\mathcal{C}_{i\alpha}^+\rangle$, where

$$|\mathcal{C}_\alpha^\pm\rangle = (|\alpha\rangle \pm |-\alpha\rangle)/\sqrt{2}\,, \tag{33a}$$

$$|\mathcal{C}_{i\alpha}^+\rangle = (|i\alpha\rangle \pm |-i\alpha\rangle)/\sqrt{2}\,. \tag{33b}$$

In the above definitions we consider cat states with large amplitudes so that the coherent states $|\pm\alpha\rangle$ $|\pm i\alpha\rangle$ are quasiorthogonal. In addition to $|\psi_0\rangle$ we introduce

$$\begin{aligned} |\psi_1\rangle &= c_g|\mathcal{C}_\alpha^-\rangle + ic_e|\mathcal{C}_{i\alpha}^-\rangle \\ |\psi_2\rangle &= c_g|\mathcal{C}_\alpha^+\rangle - c_e|\mathcal{C}_{i\alpha}^+\rangle \\ |\psi_3\rangle &= c_g|\mathcal{C}_\alpha^-\rangle - ic_e|\mathcal{C}_{i\alpha}^-\rangle\,. \end{aligned} \tag{34}$$

The subscript depicts the number of quantum jumps modulo(4) and also indicates the parity of the state. The above set of states has three properties. First, the group is closed under the action of the annihilation operator a, and whenever a quantum jump occurs state $|\psi_n\rangle$ projects to the next one, i.e. $a|\psi_n\rangle / \| a|\psi_n\rangle \| = |\psi_{(n+1)\mathrm{mod}4}\rangle$. Second, for time intervals t without jumps, $|\psi_n\rangle$ decays deterministically with $e^{-\kappa t/2}$ (see Eq. (A.37) and below). Third, keeping track of the parity $\langle\psi_n|\Pi|\psi_n\rangle = (-1)^n$, which ideally is QND measurement, reveals the number of jumps. To correct single-photon jumps one has to keep track (ideally continuously) of the parity. Therefore, one needs to keep track of the parity and pump the system to restore the dissipated energy before the amplitude of the cats becomes too small. For more on this topic see Refs[4, 18].

V. CONCLUSION

Superconducting cavities and circuits are two of the most important quantum computer building blocks for most of the proposed platforms. Harnessing their infinite-dimensional Hilbert space to store, process, and correct quantum information required a deep understanding of their features and the way they interact with other cavities or finite-level systems. We studied the creation of cat states in the strong dispersive regime and also showed a set of single and two-qubit gates one can perform by driving the system with simple control pulses. We have also introduced the Wigner quasiprobability distribution which is the phase space representation of the cavity state and it is utilized as an indicator of the (non-)classicality of the state. Next, showed how to create and stabilize cat states in a biased bath that loses photons in pairs. In the same section, we pointed out the advantages concerning error suppression, and we also utilized the quantum Zeno effect to demonstrate an X-gate. Finally, we presented a QEC code that corrects single-photon loss syndrome by measuring the parity of four orthogonal cat states. It would be interesting to study further the control of cat qubits in more complicated regimes including second order of the dispersive coupling, Kerr-nonlinearities. Also, I would like to study two-qubit gates using cat states, and bosonic error correction codes because they can be combined with cat states and propose a less resource-demanding alternative to surface codes.

Appendix: Derivations and useful formulas

For the sake of completeness and for the reader's convenience, in the following sections we gather all the needed derivations and formulas.

1. Conditional TLS rotations

The following calculation can also be found in the supplementary material of [1]. In principle, we can solve the Schrodinger equation using the Hamiltonian given in Eq. (8)

$$\frac{\partial}{\partial t}|\psi_n(t)\rangle = -\frac{i}{\hbar}\tilde{H}_n(t)|\psi_n(t)\rangle\,. \tag{A.1}$$

We can approximate the evolution for all the other photon number states $|\psi_{m\neq n}(t)\rangle$ by calculating the Dyson expansion

up to first order

$$|\psi_n(t)\rangle \approx \left\{1 - \frac{i}{\hbar}\int \mathrm{d}s\tilde{H}_n(s)\right\}|\psi_n(0)\rangle\,. \tag{A.2}$$

Consider the initial state $|\psi(0)\rangle = \sum_{n\neq m} A_n\,|g,n\rangle$ and plug it into Dyson expansion to obtain

$$\begin{aligned}
|\psi(t)\rangle &\approx \sum_{n\neq m} A_n\left\{|g,n\rangle - \frac{i}{\hbar}\int_0^t \mathrm{d}s\tilde{H}_n(s)\,|g,n\rangle\right\}\\
&= \sum_{n\neq m} A_n\Bigg\{|g,n\rangle\\
&\qquad - i\int_0^t \mathrm{d}s\epsilon(s)e^{i\Delta_{n,m}s\sigma^\dagger\sigma}\sigma_y e^{-i\Delta_{n,m}s\sigma^\dagger\sigma}\,|g,n\rangle\Bigg\}\\
&= \sum_{n\neq m} A_n\left\{|g,n\rangle - i\int_0^t \mathrm{d}s\epsilon(s)e^{i\Delta_{n,m}s\sigma^\dagger\sigma}\,|e,n\rangle\right\}\\
&= \sum_{n\neq m} A_n\left\{|g,n\rangle - i\int_0^t \mathrm{d}s\epsilon(s)e^{i\Delta_{n,m}s}\,|e,n\rangle\right\}\\
&\simeq \sum_{n\neq m} A_n\left\{|g,n\rangle - \hat{\epsilon}\left\{\Delta_{n,m}\right\}|e,n\rangle\right\}\,,
\end{aligned} \tag{A.3}$$

where $\hat{\epsilon}\{\omega = \Delta_{n,m}\}$ is the spectral component of the envelope $\epsilon(t)$ given by the Fourier transform at frequency $\Delta_{n,m}$. The normalized state after time τ is

$$|\psi(\tau)\rangle = \frac{\sum_{n\neq m} A_n\{|g,n\rangle - \hat{\epsilon}\{\Delta_{n,m}\}\,|e,n\rangle\}}{\sqrt{\sum_{n\neq m}|A_n|^2(1+\hat{\epsilon}\{\Delta_{n,m}\}^2)}}\,. \tag{A.4}$$

We will define the 'selectivity' of the TLS drive by its ability to leave all other occupied cavity states $|\psi\rangle = \sum_{n\neq m} A_n\,|g,n\rangle$ in the TLS ground state[1]. This gives the relation for selectivity [1]

$$\mathcal{S} = |\,\langle g,n|\psi(\tau)\rangle\,|^2 = \sum_{n\neq m}\frac{|A_n|^2}{\sum_{k\neq m}|A_k|^2(1+\hat{\epsilon}\{\Delta_{k,m}\}^2)}\,. \tag{A.5}$$

One can retain very high selectivity by choosing a pulse envelope with a very narrow spectral bandwidth around the driving frequency, however this comes always at the expense long gate times. This results in an approximate TLS-cavity entangling gate similar to the ideal one given in Eq. (10)

$$R^m_{\hat{y},\theta} = |m\rangle\langle m|\otimes R_{\hat{y},\theta} + \sum_{n\neq m} e^{i\xi_n}\,|n\rangle\langle n|\otimes\mathbb{1}\,, \tag{A.6}$$

with ξ_n being a photon-dependent induced phase accumulation on all every Fock state.

2. Parity operator

The photon number parity operator is defined as

$$\Pi\,|n\rangle = e^{i\pi a^\dagger a}\,|n\rangle = (-1)^n\,|n\rangle\,, \tag{A.7}$$

where $|n\rangle$ is a number state with $n = 0,1,2,3...$ photons, also known as Fock state. The parity operator can also be written using the projective operators onto the even and odd subspaces, namely

$$\Pi = \Pi_+ - \Pi_- = \sum_{n=0}|n\rangle\langle n| - \sum_{n=0}|2n+1\rangle\langle 2n+1|\,. \tag{A.8}$$

Parity operator has eigenvalue $+1$ for states with even and -1 for states with odd number of photons, respectively. One can easily show that the parity operator is hermitian, $\Pi = \Pi^\dagger$, and that it also satisfies the relation $\hat{\Pi}^2 = I$. Position and momentum operator transform under parity as follows

$$\Pi\hat{x}\Pi^{-1} = -\hat{x}\,, \tag{A.9a}$$

$$\Pi\hat{p}\Pi^{-1} = -\hat{p}\,. \tag{A.9b}$$

To prove the above relation we should first recall that

$$\hat{x} = \sqrt{\frac{\hbar}{2m\omega}}\left(a + a^\dagger\right)\,, \tag{A.10a}$$

$$\hat{p} = i\sqrt{\frac{\hbar m\omega}{2}}\left(a^\dagger - a\right)\,. \tag{A.10b}$$

With that said, we only need to show that the creation and annihilation operators obtain an minus sign when they transform under parity.

$$\begin{aligned}
\Pi a\Pi^{-1} &= e^{i\pi a^\dagger a}ae^{-i\pi a^\dagger a} = \sum_{m,n}\frac{(i\pi)^m}{m!}(a^\dagger a)^m a\frac{(-i\pi)^n}{n!}(a^\dagger a)^n\\
&= a + i\pi\left[a^\dagger a, a\right] + \frac{(i\pi)^2}{2!}\left[a^\dagger a,\left[a^\dagger a, a\right]\right] + ...\\
&= a\left(1 + i\pi + \frac{(i\pi)^2}{2!} + \frac{(i\pi)^3}{3!} + \frac{(i\pi)^4}{4!} + ...\right)\\
&= ae^{i\pi} = -a\,,
\end{aligned} \tag{A.11}$$

where we used the fact that $[a^\dagger a, a] = a$. In the same fashion, one can prove that the creation operator $a^\dagger$ transforms as $\Pi a^\dagger\Pi = -a^\dagger$. The last two results prove Eqs. (A.9).

3. Displacement operator

The displacement operator is defined as [19]

$$D(\beta) = e^{\beta a^\dagger - \beta^* a}\,, \tag{A.12}$$

where one can use the Baker–Campbell–Hausdorff formula and write the displacement operator in the following equivalent forms

$$\begin{aligned}
D(\beta) &= e^{-|\beta|^2/2}e^{\beta a^\dagger}e^{-\beta^* a}\\
&= e^{|\beta|^2/2}e^{-\beta^* a}e^{\beta a^\dagger}
\end{aligned} \tag{A.13}$$

known as *normal* and *antinormal* form. At this point we should recall that a coherent state $|\beta\rangle$ in the number state basis is written as

$$\begin{aligned}
|\beta\rangle &= e^{-|\beta|^2/2}\sum_{n=0}^{\infty}\frac{\beta^n}{\sqrt{n!}}\,|n\rangle = e^{-|\beta|^2/2}\sum_{n=0}^{\infty}\frac{\beta^n}{n!}(a^\dagger)^n\,|0\rangle\\
&= e^{-|\beta|^2/2}e^{\beta a^\dagger}\,|0\rangle = D(\beta)\,|0\rangle\,,
\end{aligned} \tag{A.14}$$

where in the second equality we used the relation that $|n\rangle = (a^\dagger)^n/\sqrt{n!}\,|0\rangle$ and in the last equality we used the fact that $e^{\lambda a}\,|0\rangle = |0\rangle$. The displacement operator obeys the semigroup relation, that is the product of two displacement operators, $D(\beta)$ and $D(\gamma)$, is the displacement operator $D(\beta+\gamma)$, up to an overall phase[20]. In detail,

$$\begin{aligned} D(\beta)D(\gamma) &= e^{\beta a^\dagger - \beta^* a} e^{\gamma a^\dagger - \gamma^* a} \\ &= e^{i\mathrm{Im}(\beta\gamma^*)} e^{(\beta+\gamma)a^\dagger - (\beta^*+\gamma^*)a} \\ &= e^{i\mathrm{Im}(\beta\gamma^*)} D(\beta+\gamma)\,, \end{aligned} \tag{A.15}$$

where to go from the first to the second line we used the Baker–Campbell–Hausdorff formula and the fact that $[\beta a^\dagger - \beta^* a, \gamma a^\dagger - \gamma^* a] = 2i\mathrm{Im}(\beta\gamma^*)$. When acting in a coherent state the overall phase is physically irrelevant [20]. It is a unitary operator, $D(\beta)^\dagger = D(-\beta) = D^{-1}(\beta)$, and displaces the creation and annihilation operators when it acts on them, namely

$$D^{-1}(\beta) a D(\beta) = a + \beta\,, \tag{A.16a}$$

$$D^{-1}(\beta) a^\dagger D(\beta) = a^\dagger + \beta^*\,. \tag{A.16b}$$

The above relations can be proved by simply using Eq. (A.15). For instance,

$$\begin{aligned} D^{-1}(\beta) a D(\beta)\,|\gamma\rangle =& D^{-1}(\beta) a\,|\gamma+\beta\rangle \\ =& D^{-1}(\beta)(\gamma+\beta)\,|\gamma+\beta\rangle \\ =& (\gamma+\beta)\,|\gamma\rangle = (a+\beta)\,|\gamma\rangle\,. \end{aligned} \tag{A.17}$$

One can also prove Eqs (A.16) by expanding the exponentials, similarly to what we did in Eq. (A.11).

We can also write the displacement operator in phase space as

$$\begin{aligned} D(X_0, P_0) &= e^{\frac{i}{2\hbar} X_0 P_0} e^{-\frac{i}{\hbar} X_0 \hat{p}} e^{\frac{i}{\hbar} P_0 \hat{x}} \\ &= e^{i\beta_R\beta_I} e^{-i\sqrt{2}\beta_R \hat{p}'} e^{i\sqrt{2}\beta_I \hat{x}'}\,, \end{aligned} \tag{A.18}$$

where in the second line we introduced the unitless position and momentum operators, $\hat{x}' = \hat{x}\sqrt{m\omega/\hbar}$ and $\hat{p}' = \hat{p}\sqrt{1/\hbar m\omega}$, respectively. Equation (A.18) also reveals the connection between displacement in the phase space and the coherent space.

Now we can underline how the displacement operator connects to the parity operator. First, we compute the projection of $D(\beta)$ in the (unitless) coordinate and momentum space, namely

$${}_x\langle x'|\, D(\beta)\,|x\rangle_x = e^{i\beta_I \frac{x'+x}{\sqrt{2}}} \delta(x - x' + \sqrt{2}\beta_R)\,, \tag{A.19a}$$

$${}_p\langle p'|\, D(\beta)\,|p\rangle_p = e^{-i\beta_R \frac{p'+p}{\sqrt{2}}} \delta(p - p' + \sqrt{2}\beta_I)\,. \tag{A.19b}$$

In both equations we used that $e^{i\lambda\hat{p}}\,|x'\rangle = |x'-\lambda\rangle$ and $e^{i\mu\hat{x}}\,|p'\rangle = |p'-\mu\rangle$, and we have already applied the δ-function on the exponentials. Second, we integrate over the real and imaginary part of the displacement to obtain

$$\int_{-\infty}^{+\infty} \mathrm{d}\beta_R D(\beta) = \sqrt{2}\pi\,|\beta_I/\sqrt{(}2)\rangle_{p\ p}\langle -\beta_I/\sqrt{(}2)|\,, \tag{A.20a}$$

$$\int_{-\infty}^{+\infty} \mathrm{d}\beta_I D(\beta) = \sqrt{2}\pi\,|\beta_R/\sqrt{(}2)\rangle_{x\ x}\langle -\beta_R/\sqrt{(}2)|\,. \tag{A.20b}$$

Finally, integrating over the whole complex plane we obtain an important relation between the displacement and parity operators

$$\frac{1}{2\pi}\int \mathrm{d}^2\beta D(\beta) = \Pi\,, \qquad \mathrm{d}^2\beta = \mathrm{d}\beta_R\,\mathrm{d}\beta_I\,. \tag{A.21}$$

The displacement operator transforms under parity

$$D(-\beta) = \Pi\hat{D}(\beta)\Pi^\dagger\,, \tag{A.22}$$

while the parity operator transforms under displacement

$$\Pi(\beta) = D(\beta)\hat{\Pi}D^\dagger(\beta) = e^{i\pi(a^\dagger - \beta^*)(a-\beta)}\,. \tag{A.23}$$

To prove the above relation, one should expand the exponential, make use of Eq. (A.16) and the fact that $D^\dagger(\beta)D(\beta) = I$. It still holds that $\Pi(\beta) = \Pi^\dagger(\beta)$ and $\Pi^2(\beta) = I$.

For purposes of completeness and future reference, we introduce the displaced number states

$$D(\gamma)\,|n\rangle = \frac{\left(a^\dagger - \gamma^*\right)^n}{\sqrt{n!}}\,|\gamma\rangle\,, \tag{A.24}$$

which is actually a coherent state. For $n = 0$ (which is also a coherent state) Eq. (A.24) leads to the Schrodinger state. In order to prove the above equation, one should write the number state in the coherent basis

$$|n\rangle = \int \mathrm{d}^2\beta\ e^{-|\beta|^2/2}\frac{(\beta^*)^n}{\sqrt{n!}}\,|\beta\rangle\,, \tag{A.25}$$

also recall that[21]

$$|\gamma\rangle = \frac{1}{\pi}\int \mathrm{d}^2\beta\ e^{\gamma\beta^* - \frac{1}{2}(|\gamma|^2+|\beta|^2)}\,|\beta\rangle\,, \tag{A.26}$$

and

$$a^\dagger\,|\beta\rangle = \left(\frac{\beta^*}{2} + \frac{\partial}{\partial\beta}\right)|\beta\rangle\,. \tag{A.27}$$

Using the last three equations and Eq. (A.15) one can easily equate the LHS with the RHS in Eq. (A.24).

4. Wigner function

The interface between the classical and quantum nature of light is elucidated by the use of Wigner distribution [19]. The Wigner function was given by Wigner in 1932

$$\begin{aligned} W(q,p) &= \frac{1}{\pi\hbar}\int_{-\infty}^{+\infty} \mathrm{d}\xi e^{-i2\xi p/\hbar}\,\langle q-\xi|\,\rho\,|q+\xi\rangle \\ &= \frac{1}{\pi\hbar}\int_{-\infty}^{+\infty} \mathrm{d}\zeta e^{+i2\zeta q/\hbar}\,\langle p-\zeta|\,\rho\,|p+\zeta\rangle\,. \end{aligned} \tag{A.28}$$

However, it can be proved that the Wigner function is actually the expectation value of the displaced parity operator [22]

$$\begin{aligned} W(q,p) = \frac{2}{\pi}\mathrm{Tr}\left\{\rho\Pi(\beta)\right\} &= \frac{2}{\pi}\mathrm{Tr}\left\{\rho D^\dagger(-\beta)\Pi D(-\beta)\right\} \\ &= \frac{1}{\pi\hbar}\mathrm{Tr}\left\{\rho D(q,p)\Pi D^\dagger(q,p)\right\}\,. \end{aligned} \tag{A.29}$$

The Wigner function is a quasi-probability distribution. Unlike wave functions, it is guaranteed to be real, but unlike classical probabilities, it can be negative [13]. In quantum optics, states with negative-valued Wigner function are defined to have quantum states, or 'non-classical'.

Since it is a (quasi)probability distribution, Wigner function must integrate to unity

$$\begin{aligned}\int \mathrm{d}\beta^2\ W(\beta) &= \frac{2}{\pi}\iint \mathrm{d}\beta_R \mathrm{d}\beta_I \mathrm{Tr}\left\{\rho\hat{\Pi}(\beta)\right\} \\ &= \mathrm{Tr}\left\{\rho\Pi\frac{2}{\pi}\iint \mathrm{d}\beta_R \mathrm{d}\beta_I D(-2\beta)\right\} \\ &= \mathrm{Tr}\left\{\rho\Pi\Pi\Pi\right\} = \mathrm{Tr}\left\{\rho I\right\} = 1\end{aligned} \tag{A.30}$$

An extensive discussion on the Wigner function in the P-,Q- and R- representations can be found in Refs [19, 21].

Next, we present the Wigner distribution for specific examples. First, we consider a coherent state where $\rho = |\alpha\rangle\langle\alpha| = \int \mathrm{d}^2\xi P(\xi)|\xi\rangle\langle\xi|$ and $P(\xi) = \delta^{(2)}(\xi-\alpha) = \delta(\xi_R-\alpha_R)\delta(\xi_I-\alpha_I)$ with the Wigner function being

$$\begin{aligned}W(\beta)\frac{\pi}{2} &= \mathrm{Tr}\left\{\hat{D}(-\beta)\rho\hat{D}^\dagger(-\beta)\hat{\Pi}\right\} \\ &= \int \mathrm{d}^2\xi\, P(\xi)\langle\xi|\hat{D}^\dagger(-\beta)\hat{\Pi}\hat{D}(-\beta)|\xi\rangle \\ &= \int \mathrm{d}^2\xi\, P(\xi)\langle\xi-\beta|-\xi+\beta\rangle = \int \mathrm{d}^2\xi\, P(\xi)e^{-2|\xi-\beta|^2} \\ &= e^{-2|\alpha-\beta|^2} \Rightarrow \\ W(\beta) &= \frac{2}{\pi}e^{-2|\alpha-\beta|^2}.\end{aligned} \tag{A.31}$$

In this case, the Wigner function is a Gaussian distribution centered at (α_R, α_I), see Fig. 3(a).

In the case of a Fock state $\rho = |n\rangle\langle n|$ the Wigner function is given[21]

$$W(\beta) = \frac{2}{\pi}(-1)^n e^{-2|\beta|^2} L_n\left(4|\beta|^2\right), \tag{A.32}$$

where $L_n(x)$ are the Laguerre polynomial. In particular, for $n = 1$ we have

$$W(\beta) = \frac{2}{\pi}e^{-2|\beta|^2}\left(4|\beta|^2 - 1\right), \tag{A.33}$$

which is clearly negative in the vicinity of $|\beta| = 0$, and at $\beta = 0$ Wigner function gets the lowest possible value $W(0) = -2/\pi$, see Fig. 3(c-d). In contrast to the ground state $n = 0$, the negative values of the Wigner function of a number state $n > 0$ signify the highly non-classical character of the corresponding state.

For the sake of completeness, we shall also include the Wigner function for the thermal or chaotic light

$$W(\beta) = \frac{1}{\pi}\frac{1}{\bar{n}+1}e^{-\frac{|\beta|^2}{\bar{n}+1/2}}, \tag{A.34}$$

where $\bar{n} = (e^{\hbar\omega/(k_B T)} - 1)^{-1}$ is the mean thermal photon number. The above distribution is always positive, see Fig. 3(b) The derivation is straightforward and can be found in [19, 21].

Now let's derive the Wigner function for cat state defined as $|\mathcal{C}^\pm\rangle = \mathcal{N}_\pm(|\alpha\rangle \pm |-\alpha\rangle)$, or in terms of density matrix

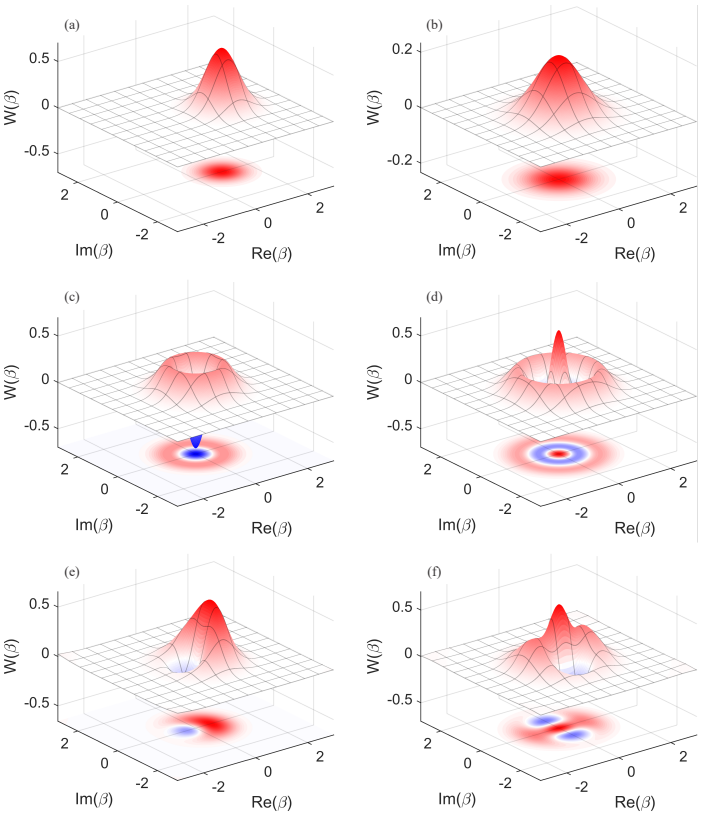

FIG. 3. Wigner functions and their footprints for different field states. (a) Coherent state $|\alpha = 1\rangle$, (b) thermal field with average photon number $\bar{n} = 1/2$, (c) number state $|n = 1\rangle$, (d) $|n = 2\rangle$, (e) $|\psi\rangle = (|0\rangle + |1\rangle)/\sqrt{2}$, and (f) $|\psi\rangle = (|0\rangle + |2\rangle)/\sqrt{2}$. Red and blue colors represent positive and negative values, respectively.

$\rho_\pm = |\mathcal{C}^\pm\rangle\langle\mathcal{C}^\pm|$. We start from Eq. (A.29) and we calculate the expectation value of the displaced parity operator in the following fashion

$$\begin{aligned}W(\beta) &= \frac{2}{\pi}\mathrm{Tr}\left\{\rho D^\dagger(-\beta)\Pi D(-\beta)\right\} \\ &= \frac{2}{\pi}\left(\mathcal{N}_\pm\right)^2\langle\mathcal{C}^\pm|D^\dagger(-\beta)\Pi D(-\beta)|\mathcal{C}^\pm\rangle \\ &= \frac{2}{\pi}\left(\mathcal{N}_\pm\right)^2 e^{-2|\beta|^2}\Big[e^{-2|\beta+\alpha|^2} + e^{-2|\beta-\alpha|^2} \\ &\qquad \pm e^{i4\mathrm{Im}(\alpha^*\beta)} \pm e^{-i4\mathrm{Im}(\alpha^*\beta)}\Big] \\ &= \frac{4}{\pi}\left(\mathcal{N}_\pm\right)^2 e^{-2|\beta|^2}\Big[\cosh\left(4\alpha\mathrm{Re}\left(\beta\right)\right)e^{-2\alpha^2} \\ &\qquad \pm \cos\left(4\alpha\mathrm{Im}\left(\beta\right)\right)\Big],\end{aligned} \tag{A.35}$$

where the first two terms come from the diagonal part of the density matrix, while the last two originate from the off-diagonal terms. To derive the above result, we used Eqs. (A.15),(A.22), and $\hat{\Pi}|\zeta\rangle = |-\zeta\rangle$. In the last step we took α to be real, for simplicity. The even and odd cat Wigner functions are plotted in Fig. 4.

5. Master equation

In this section, we present the master equation of a cavity field coupled to a reservoir of infinite harmonic oscillators

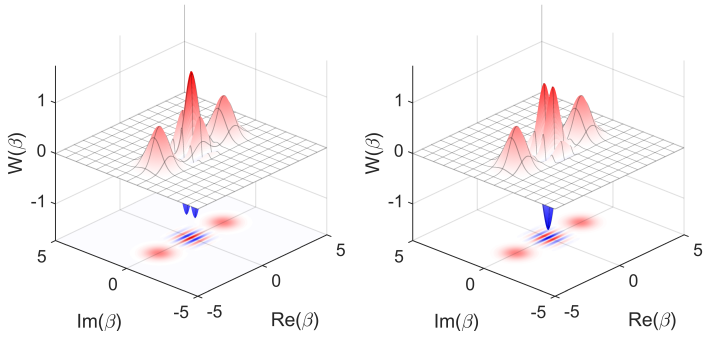

FIG. 4. Wigner functions and their footprints for (a) even and (b) odd cat state. A cat state is defined as $|\mathcal{C}^{\pm}\rangle = \mathcal{N}_{\pm}(|\alpha\rangle \pm |-\alpha\rangle)$. Here $\alpha = 2.5$ and $\mathcal{N}_{\pm} = [2(1 \pm e^{-2|\alpha|^2})]^{-1/2} \simeq 1/\sqrt{2}$.

resulting in the field relaxation, also known as a leaky cavity. The system Hamiltonian is $H_S = \hbar\omega a^\dagger a$, while the reservoir is given by $H_R = \sum_k \hbar\omega_k b_k^\dagger b_k$. Considering the Markovian approximation for the reservoir, one can show the master equation for the reduced density matrix of the cavity field $\tilde{\rho}_S$ is [21]

$$\frac{\partial}{\partial_t}\tilde{\rho}_S = -i\left[\omega a^\dagger a, \rho_S\right] + \frac{1}{2}\kappa(1+\bar{n})\left(2a\tilde{\rho}_S a^\dagger - a^\dagger a\tilde{\rho}_S - \tilde{\rho}_S a^\dagger a\right) + \frac{1}{2}\kappa\bar{n}\left(2a^\dagger\tilde{\rho}_S a - aa^\dagger\tilde{\rho}_S - \tilde{\rho}_S aa^\dagger\right), \tag{A.36}$$

where $\bar{n} \equiv \bar{n}(\omega)$ is the mean number of thermal photons at the cavity frequency, and κ is the decay rate of the cavity mode [21]. Note that the number of thermal photons depends on the temperature T of the bath, and in the low-temperature limit (i.e.$k_B T \ll \hbar\omega$) $\bar{n} \to 0$. Hence, Eq. (A.36) yields to

$$\frac{\partial}{\partial_t}\tilde{\rho}_S = -i\left[\omega_0 a^\dagger a, \rho_S\right] + \frac{1}{2}\kappa\left(2a\tilde{\rho}_S a^\dagger - a^\dagger a\tilde{\rho}_S - \tilde{\rho}_S a^\dagger a\right), \tag{A.37}$$

which describes the relaxation of the cavity field into the empty thermal bath. The above approximation is relevant since most of the cavity-/circuit-QED experiments are conducted at few mK [1, 7].

The master equation given above, Eq. (A.37), can be used to calculate the expectation value of various operators. However, due to its specific form, we observe that it behaves like an equation of motion for a coherent state. More specifically, consider the cavity field in the state $|\beta\rangle = \hat{D}(\beta)|0\rangle$, or equivalently $\rho_\beta = |\beta\rangle\langle\beta|$. For a perfect cavity without leakage the expansion in time is given $|\beta(t)\rangle = |\beta e^{-i\omega_0 t}\rangle$, while in the case of relaxation we obtain $|\beta(t)\rangle = |\beta e^{-i\omega_0 t - \kappa t/2}\rangle$. In both cases the state remains coherent, but in the latter it also decays exponentially. The last result reveals that Eq. (A.37) has very specific pure states as solutions, which means that $\rho_S(t)$ remains pure in time.

Now let's go one step further and consider a pure state $\rho_S(0) = |\psi_0\rangle\langle\psi_0|$ where $|\psi_0\rangle = \mathcal{N}(|\beta_1\rangle + |\beta_2\rangle)$, with $\mathcal{N}^{-2} = 2(1 + \mathrm{Re}\{\exp(-|\beta_1|^2/2 - |\beta_2|^2/2 + \beta_1\beta_2^*)\})$ the normalization factor. We plug the density operator into Eq. (A.37) to obtain the following set of differential equations

$$\frac{\dot{\beta}_1}{\beta_1} = -i\omega_0 - \kappa/2\,, \tag{A.38a}$$

$$\frac{\dot{\beta}_2}{\beta_2} = -i\omega_0 - \kappa/2\,, \tag{A.38b}$$

$$\frac{\dot{f}}{f} = \frac{1}{2}\frac{\partial}{\partial t}\left(|\beta_1|^2 + |\beta_2|^2 + \kappa\beta_1\beta_2^*\right), \tag{A.38c}$$

where the first two are identical and refer to diagonal terms, while last one refers to off-diagonal term. We skip the first two equations since we have already shown and explained their solutions and we move on to the third one. Equation (A.38c) obtains the solution

$$f = \exp\left[\left(1 - e^{-\kappa t}\right)\left(-\frac{|\beta_1|^2}{2} - \frac{|\beta_2|^2}{2} + \beta_1\beta_2^*\right)\right]. \tag{A.39}$$

Note that for small times ($\kappa t \ll 1$) the first part of the exponential yields to $1 - e^{-\kappa t} \simeq -\kappa t$ and thus the amplitude of the coherence is determined by

$$|f| \simeq e^{-\frac{1}{2}\kappa t|\beta_1 - \beta_2|^2} = e^{-\frac{1}{2}\kappa t\mathcal{S}}\,, \tag{A.40}$$

which decays with rate analogous to the size $\mathcal{S} = |\beta_1 - \beta_2|^2$ of the cat, namely $\kappa t\mathcal{S}/2$, and for well separated coherent states ($\mathcal{S} \gg 1$) this rate is much larger than κ. In particular, the decoherence time is given $T_2 = (\kappa\mathcal{S}/2)^{-1} = T_1 2/\mathcal{S}$, where $T_1 = 1/\kappa$ is the characteristic decay time. The decoherence in macroscopically distinct states is incredibly faster compared to κ, and thus too fast to be observed [23]. Recall that in purely microscopic systems, like two-level systems, the populations decay with rate γ and the coherences with $\gamma/2$, not much different and in fact smaller.

For sake of completeness, the density matrix at time $t \geq 0$ is

$$\rho_S(t) = \mathcal{N}^2\Big(|\beta_1(t)\rangle\langle\beta_1(t)| + |\beta_2(t)\rangle\langle\beta_2(t)| + f(t)|\beta_1(t)\rangle\langle\beta_2(t)| + f^*(t)|\beta_2(t)\rangle\langle\beta_1(t)|\Big). \tag{A.41}$$

[1] B. Vlastakis, G. Kirchmair, Z. Leghtas, S. E. Nigg, L. Frunzio, S. M. Girvin, M. Mirrahimi, M. H. Devoret, and R. J. Schoelkopf, Deterministically encoding quantum information using 100-photon schrödinger cat states, Science **342**, 607 (2013).

[2] A. Wallraff, D. I. Schuster, A. Blais, L. Frunzio, R.-S. Huang, J. Majer, S. Kumar, S. M. Girvin, and R. J. Schoelkopf, Strong coupling of a single photon to a superconducting qubit using circuit quantum electrodynamics, Nature **431**, 162–167 (2004).

[3] D. Gottesman, A. Kitaev, and J. Preskill, Encoding a qubit in an oscillator, Phys. Rev. A **64**, 012310 (2001).

[4] Z. Leghtas, G. Kirchmair, B. Vlastakis, R. J. Schoelkopf, M. H. Devoret, and M. Mirrahimi, Hardware-efficient autonomous quantum memory protection, Phys. Rev. Lett. **111**, 120501 (2013).

[5] S. Haroche and J.-M. Raimond, *Exploring the Quantum* (Oxford University Press, 2006).

[6] J. Guillaud, J. Cohen, and M. Mirrahimi, Quantum computation with cat qubits, SciPost Physics Lecture Notes 10.21468/scipostphyslectnotes.72 (2023).

[7] Z. Leghtas, S. Touzard, I. M. Pop, A. Kou, B. Vlastakis, A. Petrenko, K. M. Sliwa, A. Narla, S. Shankar, M. J. Hatridge, M. Reagor, L. Frunzio, R. J. Schoelkopf, M. Mirrahimi, and M. H. Devoret, Confining the state of light to a quantum manifold by engineered two-photon loss, Science **347**, 853–857 (2015).

[8] R. Lescanne, M. Villiers, T. Peronnin, A. Sarlette, M. Delbecq, B. Huard, T. Kontos, M. Mirrahimi, and Z. Leghtas, Exponential suppression of bit-flips in a qubit encoded in an oscillator, Nature Physics **16**, 509–513 (2020).

[9] J. Guillaud and M. Mirrahimi, Repetition cat qubits for fault-tolerant quantum computation, Phys. Rev. X **9**, 041053 (2019).

[10] We refer to the physical qubit as TLS to avoid the confusion between the logical and the Cat qubits we introduce later on.

[11] A. Blais, R.-S. Huang, A. Wallraff, S. M. Girvin, and R. J. Schoelkopf, Cavity quantum electrodynamics for superconducting electrical circuits: An architecture for quantum computation, Phys. Rev. A **69**, 062320 (2004).

[12] S. M. Girvin, Circuit QED: superconducting qubits coupled to microwave photons, in *Quantum Machines: Measurement and Control of Engineered Quantum Systems* (Oxford University PressOxford, 2014) pp. 113–256.

[13] S. M. Girvin, Schrodinger cat states in circuit qed (2017).

[14] S. Touzard, A. Grimm, Z. Leghtas, S. O. Mundhada, P. Reinhold, C. Axline, M. Reagor, K. Chou, J. Blumoff, K. M. Sliwa, S. Shankar, L. Frunzio, R. J. Schoelkopf, M. Mirrahimi, and M. H. Devoret, Coherent oscillations inside a quantum manifold stabilized by dissipation, Phys. Rev. X **8**, 021005 (2018).

[15] R. J. Glauber, Coherent and incoherent states of the radiation field, Phys. Rev. **131**, 2766 (1963).

[16] S. Puri, L. St-Jean, J. A. Gross, A. Grimm, N. E. Frattini, P. S. Iyer, A. Krishna, S. Touzard, L. Jiang, A. Blais, S. T. Flammia, and S. M. Girvin, Bias-preserving gates with stabilized cat qubits, Science Advances **6**, 10.1126/sciadv.aay5901 (2020).

[17] M. Mirrahimi, Z. Leghtas, V. V. Albert, S. Touzard, R. J. Schoelkopf, L. Jiang, and M. H. Devoret, Dynamically protected cat-qubits: a new paradigm for universal quantum computation, New Journal of Physics **16**, 045014 (2014).

[18] N. Ofek, A. Petrenko, R. Heeres, P. Reinhold, Z. Leghtas, B. Vlastakis, Y. Liu, L. Frunzio, S. M. Girvin, L. Jiang, M. Mirrahimi, M. H. Devoret, and R. J. Schoelkopf, Extending the lifetime of a quantum bit with error correction in superconducting circuits, Nature **536**, 441–445 (2016).

[19] M. O. Scully and M. S. Zubairy, *Quantum Optics* (Cambridge University Press, 1997).

[20] C. Gerry and P. Knight, *Introductory Quantum Optics* (Cambridge University Press, 2004).

[21] P. Lambropoulos and D. Petrosyan, *Fundamentals of Quantum Optics and Quantum Information* (Springer Berlin Heidelberg, 2007).

[22] A. Royer, Wigner function as the expectation value of a parity operator, Phys. Rev. A **15**, 449 (1977).

[23] L. Davidovich, M. Brune, J. M. Raimond, and S. Haroche, Mesoscopic quantum coherences in cavity qed: Preparation and decoherence monitoring schemes, Phys. Rev. A **53**, 1295 (1996).